Assessment of Divertor Heat Load with and without External Magnetic Perturbation

B. Sieglin[1], T. Eich[1], M. Faitsch[1], A. Herrmann[1], A. Kirk[2], A. Scarabosio[1], W. Suttrop[1], A. Thornton[2], JET contributors* , EUROFusion MST1 Team† and ASDEX Upgrade Team[1]

[1]Max-Planck-Institut für Plasmaphysik, Boltzmannstraße 2, D-85748 Garching, Germany
[2]CCFE, Culham Science Centre, Oxfordshire OX14 3DB, United Kingdom
*EUROfusion Consortium, JET, Culham Science Centre, Abingdon, OX14 3DB, UK

Corresponding Author: Bernhard.Sieglin@ipp.mpg.de

Abstract:
Divertor heat load is a major concern for large scale fusion devices such as ITER. Both steady state heat exhaust as well as heat loads due to transient events such as type-I ELMs need to be understood in order to predict the thermal load onto the divertor targets. The use of external magnetic perturbation to mitigate the ELM induced divertor load has been topic of a multitude of studies In this study the influence of external magnetic perturbation on the SOL heat transport in ASDEX Upgrade L-Mode is shown. It is found that the heat transport perpendicular to the magnetic field is within the uncertainty unaffected by external magnetic perturbation. The influence of external magnetic perturbation on the ELM deposited energy density is shown. A scaling coupling the ELM deposited energy density with the upstream pedestal pressure is available. This scaling is able to describe the observed reduction of the ELM deposited energy density with external magnetic perturbation as a loss in pedestal pressure.

1 Introduction

Divertor heat load is a major concern for large scale fusion devices such as ITER [1, 2, 3]. Both steady state heat exhaust as well as heat loads due to transient events such as type-I ELMs need to be understood in order to predict the thermal load onto the divertor targets. In recent years ELM mitigation using external magnetic perturbation has been subject to intensive research. In this paper the influence of external magnetic perturbation is studied in both L- and H-Mode.

To study the influence of magnetic perturbation on the heat transport in the scrape-off layer (SOL) discharges in ASDEX Upgrade L-Mode conditions are used. In contrast to H-Mode, L-Mode does not exhibit large transient events such as ELMs and therefore offers more stable divertor and SOL conditions. For the power fall-off length λ_q in ASDEX

*See the author list of Overview of the JET results in support to ITER by X. Litaudon et al. to be published in Nuclear Fusion Special issue: overview and summary reports from the 26th Fusion Energy Conference (Kyoto, Japan, 17-22 October 2016)

†See http://www.euro-fusionscipub.org/mst1

Upgrade L-Mode a scaling is available [4] which has a similar parametric dependence as the widely agreed multi machine scaling for H-Mode [5], but with a larger absolute scale. The divertor broadening S in ASDEX Upgrade L-Mode is described by perpendicular heat diffusion in the divertor with parallel electron conduction [4].

With the application of external magnetic perturbation the target heat flux profiles ceases to be axisymmetric and a characteristic heat flux pattern is induced [6]. Due to the absence of transient events in L-Mode it is possible to measure the full 2D heat flux profile on the divertor target by a rigid rotation of the external magnetic perturbation. Observing the full heat flux distribution enables the investigation of the influence of the magnetic perturbation on the global SOL and divertor heat transport.

2 L-Mode Heat Transport

In order to investigate the influence of external magnetic perturbation, the heat transport in absence of magnetic perturbation needs to be examined.

The toroidal symmetric target heat load profile, in dependence of the poloidal target location s, is described by an exponential decay with the power fall-off length λ_q and a diffusive broadening in the divertor region S [5].

$$q(s) = \frac{q_0}{2} \exp\left(\left(\frac{S}{2\lambda_q}\right)^2 - \frac{s}{\lambda_q f_x}\right) \cdot \operatorname{erfc}\left(\frac{S}{2\lambda_q} - \frac{s}{S f_x}\right) \tag{1}$$

This model has been used successfully to describe steady heat flux profiles in both L- and H-Mode [7, 8, 9, 10, 11, 12, 4]. Figure 1 shows the measured heat flux profiles for ASDEX Upgrade L-Mode conditions for different plasma densities at a plasma current of $I_p = 1.0$ MA and a toroidal magnetic field of $B_{tor} = -2.5$ T. The heat flux is normalized to the peak heat flux expected without divertor broadening S. It is seen that the heat flux model (Equation 1) describes the observed heat flux profiles within the measurement noise.

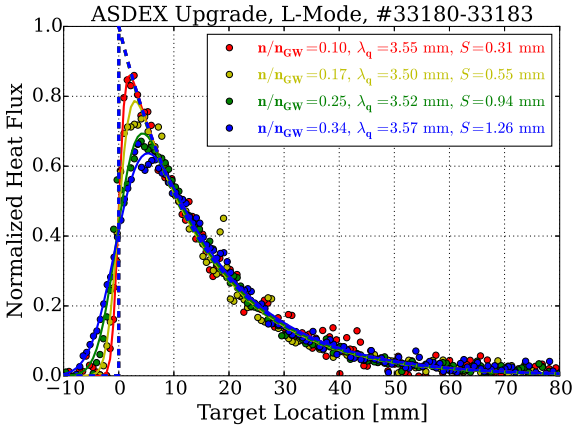

FIG. 1: Normalized target heat flux profiles for the outer divertor target for different plasma densities (circles = measurement, solid lines = Fitted Model, dashed lines = Reconstructed heat flux without divertor broadening).

For H-Mode conditions an empirical scaling based on a multi machine database exists [9] which predicts $\lambda_q \leq 1.0$ mm. For L-Mode conditions a study using ASDEX Upgrade L-Mode [4] has made a similar scaling.

$$\text{L-Mode} \quad \lambda_q\,[\text{mm}] = 1.45 \pm 0.13 \quad B_{tor}^{-0.78} \cdot q_{cyl}^{1.07\pm0.07} \cdot P_{SOL}^{-0.14\pm0.05} \tag{2}$$

$$\text{H-Mode} \quad \lambda_q\,[\text{mm}] = 0.73 \pm 0.38 \quad B_{tor}^{-0.78\pm0.25} \cdot q_{cyl}^{1.20\pm0.27} \cdot P_{SOL}^{0.10\pm0.11} \cdot R^{0.02\pm0.20} \tag{3}$$

In the L-Mode scaling the exponent for the toroidal magnetic field B_{tor} is taken fixed from the H-Mode scaling since no significant variation of B_{tor} is available in the L-Mode data. The dependence on the cylindrical safety factor c_{cyl} is within the uncertainty identical to the H-Mode scaling. The dependence on the power crossing the separatrix into the SOL P_{SOL} shows a different behaviour compared to the H-Mode scaling. It is slightly negative, whereas the H-Mode scaling has a positive dependence, which however is zero within the uncertainty. Most notably in the scaling the prefactor is more or less exactly a factor of two larger for L-Mode compared to H-Mode. Empirically this confirms the observation that the power load footprint in L-Mode is about twice as large compared to H-Mode. It is however noteworthy that the parametric dependence for both L- and H-Mode are similar despite their significant differences in the edge heat transport (e.g. formation of a edge transport barrier).

In the next section the SOL heat transport is studied in the presence of external magnetic perturbation.

3 Influence of External Magnetic Perturbation on Steady State SOL Heat Transport

In this section the influence of magnetic perturbation on the heat transport in the SOL and the resulting heat load pattern on the divertor target is investigated in ASDEX Upgrade L-Mode with low recycling attached divertor conditions.

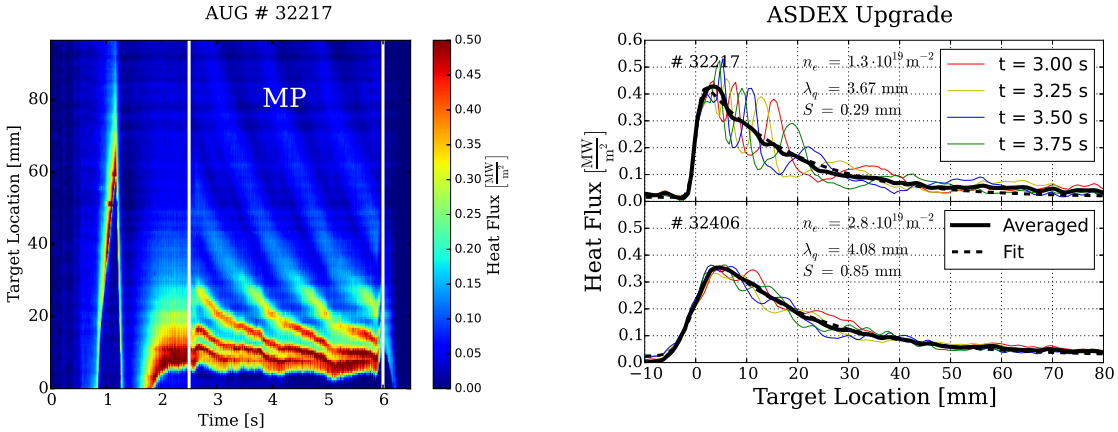

(a) Divertor target heat flux pattern without ($t = 2.0 - 2.5$ s) and with rotating resonant magnetic perturbation ($t > 2.5$s) for low density ($n/n_{GW} = 0.15$).

(b) Divertor target heat flux profile with resonant magnetic perturbation for low ($n/n_{GW} = 0.15$, top panel) and medium density ($n/n_{GW} = 0.3$, bottom panel).

FIG. 2: Measured target heat flux patterns with magnetic perturbation in ASDEX Upgrade. The characteristic lobe structure becomes less pronounced with increasing density.

ASDEX Upgrade is equipped with two toroidal rows of eight saddle coils, which are above and below the outer midplane [13, 14]. In the experiments presented here a pertur-

bation with a toroidal mode number $n = 2$ are used. The power supply of the saddle coils in ASDEX Upgrade allows the rigid rotation of the external magnetic perturbation with arbitrary phase between the upper and lower row [15, 16]. This enables the measurement of the full 2D heat flux pattern on the divertor structure with an IR system [17] at a fixed position. In the experiment the external magnetic perturbation is rotated with 1 Hz. The rotation frequency is chosen such, to complete at least two full rotations within the discharge and to minimize the screening due to the passive support loop (PSL) of ASDEX Upgrade.

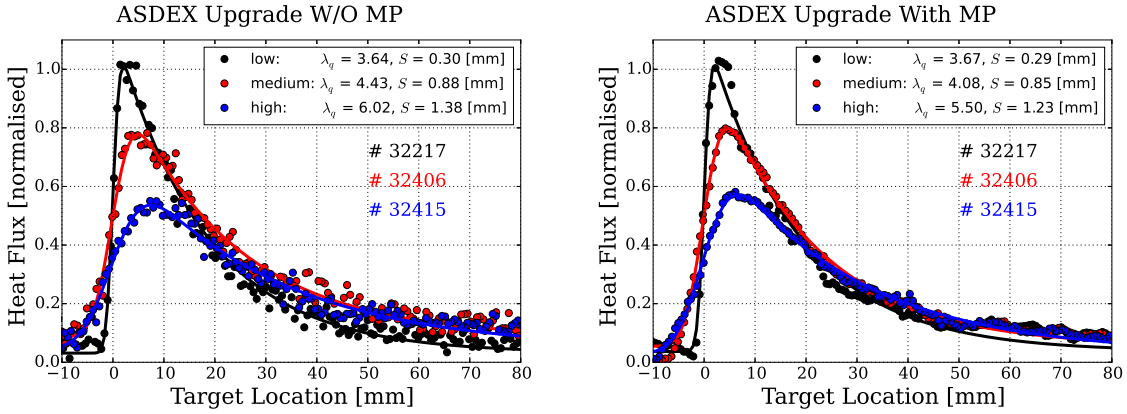

(a) Target heat flux profiles without external magnetic perturbation for different plasma densities.

(b) Toroidal averaged target heat flux profiles with external magnetic perturbation for different plasma densities.

FIG. 3: Target heat flux profiles with and without external magnetic perturbation for different density levels.

Figure 2(a) shows the time evolution of the target heat flux profile for the outer divertor during a low density L-Mode discharge with a resonant n=2 magnetic perturbation. The resulting heat flux distribution on the divertor target is not toroidally uniform and leads to a local increase of the heat flux. This 2D structure has been reported on many devices studying external magnetic perturbation [18, 19, 20, 21, 6].

Figure 2(b) shows the target heat flux profile for different times, corresponding to different phases of the applied external magnetic perturbation, for a low and medium density discharge. The toroidal averaged target heat flux profile (black) is the same as the profile in the axis-symmetric case without external magnetic perturbation, the power fall-off length λ_q does not significantly increase with the magnetic perturbation. The observed heat flux pattern is explained by heat flux calculations using the vacuum field of the external magnetic perturbation [6]. It is seen that the intensity of the lobes is reduced with increasing divertor broadening S.

Figure 3 shows the target heat flux profiles without external magnetic perturbation (FIG. 3(a)) and the toroidal averaged heat flux profiles with external magnetic perturbation (FIG. 3(b)) for different density level. It is seen that both λ_q and S have similar values for the different density levels, independent on the presence of external magnetic

perturbation. From this it is concluded that the perpendicular heat transport in the SOL and divertor region are not changed by the external magnetic perturbation.

The toroidal asymmetry of the heat flux is quantified by the toroidal peaking which is defined by the ratio of the peak heat flux and the toroidal averaged heat flux.

Figure 4 shows the measured (red) and modelled (black) toroidal peaking of the divertor target heat flux. It is seen that the peaking is reduced with increasing divertor broadening S, which is consistent with the observation that the characteristic of the observed lobe structure is reduced with increasing density. The modelling using the vacuum field approach [6] is able to reproduce the observed toroidal peaking in both trend and absolute magnitude. Already a moderate broadening is sufficient to reduce the toroidal peaking significantly approaching the unperturbed heat flux profile for larger S. This observation needs to be studied in further detail, also including H-Mode, since the induced toroidal peaking is a concern for the application of external magnetic perturbation in ITER. It is yet unclear if in a partially detached state, as is foreseen for ITER operation, the toroidal peaking will still be prominent or if S will be sufficiently large to mitigate the toroidal peaking.

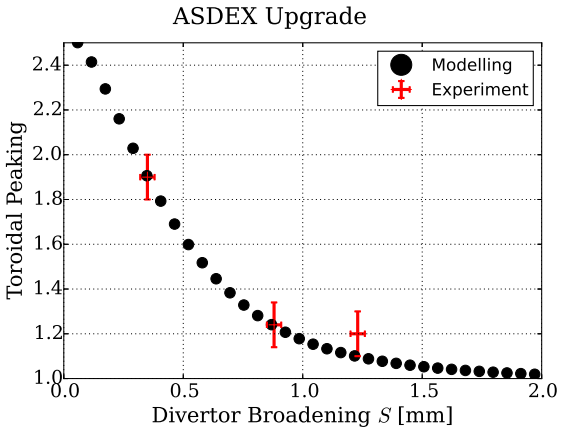

FIG. 4: Measured (red) and modelled (black) toroidal peaking of the target heat flux, one λ_q away from the separatrix, in dependence of the divertor broadening S [6].

4 ELM Induced Divertor Load

The mitigation of ELM induced divertor load is the main objective for the application of external magnetic perturbation in ITER. Extensive studies have been performed to scale and predict the ELM induced divertor load towards large fusion devices. Recent attempts are using the pedestal pressure as the main quantity to scale the parallel ELM deposited energy density [22], also known as ELM energy fluence, $\epsilon_{||}$. A simple model has been derived which is able to describe the observed $\epsilon_{||}$ in ASDEX Upgrade, JET and MAST.

$$\epsilon_{||} = \Delta_{\text{equi}} \cdot 2\pi a \cdot \sqrt{\frac{1+\kappa^2}{2}} \cdot \frac{3}{2} \cdot n_{e,ped} \cdot k_b \cdot T_{e,ped} \cdot \frac{B_{\text{tor}}}{B_{\text{pol}}} \tag{4}$$

Where Δ_{equi} is a geometry factor derived by comparison to the real equilibrium reconstruction, which is ~ 1.9 for ASDEX Upgrade, a is the minor radius, κ the elongation, $n_{e,ped}$ and $T_{e,ped}$ the electron density and temperature at the pedestal top. B_{tor} and B_{pol} are the toridal and polidal magnetic field. To illustrate the effect of external magnetic perturbation on the ELM induced divertor load the ASDEX Upgrade discharge #32080

is used. The discharge operated at a toroidal magnetic field of $B_{tor} = -2.5$ T with a plasma current of $I_p = 0.8$ MA and auxiliary heating of $P_{aux} \approx 7.5$ MW.

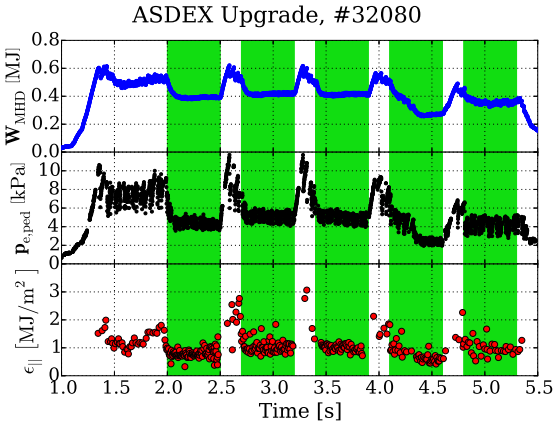

(a) Timetrace of the stored energy (blue), pedestal electron pressure (black) and deposited energy fluence at the outer divertor target (red) for ASDEx Upgrade discharge #32080. The green areas indicate the times when external magnetic perturbation was switched on.

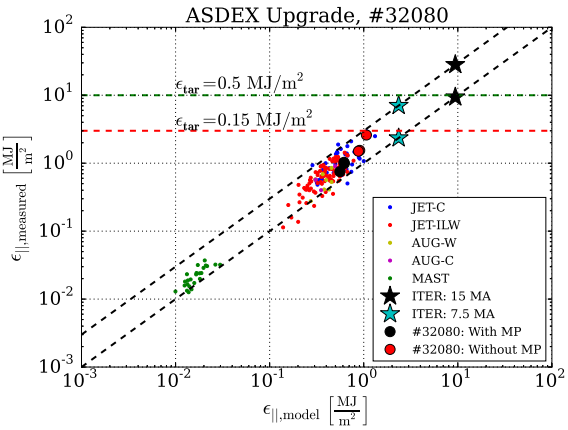

(b) Measured parallel ELM energy fluence in dependence on the predicted ELM energy fluence (Equation 4) for the available data from ASDEX Upgrade, MAST and JET [22] and for ASDEX Upgrade discharge #32080. The model prediction (with factor 3 scatter) is given as black dashed lines. The material limits are indicated as horizontal lines.

FIG. 5: Influence of external magnetic perturbation on pedestal pressure and ELM energy fluence in ASDEX Upgrade discharge #32080. The observed ELM energy fluence is compared to the prediction (Equation 4) und existing data from ASDEX Upgrade, MAST and JET.

Figure 5(a) shows the timetrace of the stored energy W_{MHD} (blue), pedestal electron pressure $p_{\mathrm{e,ped}}$ (black) and the ELM induced parallel energy fluence $\epsilon_{||}$ (red). The green shaded areas indicate the periods in the discharge with active external magnetic perturbation. It is seen that all three quantities are reduced during phases with external magnetic perturbation compared to unperturbed phases. The reduction of ELM induced energy fluence $\epsilon_{||}$ is correlated to the reduction of the pedestal pressure $p_{\mathrm{e,ped}}$ and the reduction of the stored energy W_{MHD}.

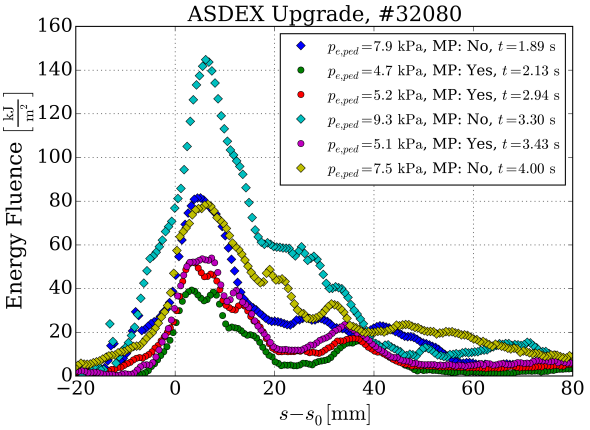

FIG. 6: Oberved ELM deposited target energy fluence for ASDEX Upgrade #32080 with and without external magnetic perturbation.

Figure 5(b) shows the measured parallel ELM energy fluence in comparison to the model prediction (Equation 4). Available data from ASDEX Upgrade, MAST and

JET [22] are shown as dots. The measured data from ASDEX Upgrade discharge #32080 is shown as circles. It is seen that both cases with and without external magnetic perturbation are captured within the prediction of the model. The observed reduction of the ELM energy fluence in the presence of external magnetic perturbation is explained by the reduction in pedestal pressure. Studies for ELM mitigation should correct the assessment of mitigation for the reduction of the pedestal pressure. The observed scatter of $\epsilon_{||}$ of about a factor of three is consistent with the scatter of $\sqrt{E}$ in the data. Together with a change of a factor of two in the pedestal pressure this is sufficient to explain the reported factor of six in ELM mitigation studies [23].

The ELM deposited energy fluence ϵ_{tar} for the outer divertor target is shown in figure 6. Without external magnetic perturbation the peaks in ϵ_{tar} appear in a statistic manner on the divertor target, giving averaged over multiple ELMs a smooth profile [22]. In contrast to this the peaks appear, preferentially, in the same location with external magnetic perturbation [24]. The ELM *locks* to the external perturbation, therefore a rotation of the external magnetic perturbation is required to measure the whole 2D pattern of the ELM. This needs to be taken into account when comparing phases with and without external magnetic perturbation, since it is possible that the highest loaded area is not captured since it could occur in a different toroidal location than the area observed.

5 Conclusions

It is shown in this paper that the target heat flux profile on the outer divertor target in ASDEX Upgrade L-Mode is described by the same model used for the study of the heat flux profile in Inter-ELM H-Mode. Furthermore the parametric dependence of λ_q is similar to the empirical multi machine scaling for H-Mode, differing in the prefactor by a factor of two and a negative SOL heating power dependence for L-Mode. The negative dependence on the SOL heating power of the L-Mode scaling compared to the, within the uncertainty independent H-Mode scaling, could be explained by a dependence of λ_q on the separatrix temperature which is found in the L-Mode data.

The measurement of the full 2D divertor target heat load pattern with external magnetic perturbation show the non axisymmetric nature of the heat flux. The magnetic perturbation induces local deviation from the axisymmetric heat flux which is reduced with increasing divertor broadening S. The toroidal averaged heat flux profiles are, within the uncertainty, identical to the heat flux profiles observed without magnetic perturbation. From this it is concluded that the parallel and perpendicular heat transport in L-Mode is unaffected by magnetic perturbation, the heat flux pattern itself is described by a simple model using the vacuum field approach coupled with the two point model in the SOL [6].

The application of external magnetic perturbation in ASDEX Upgrade H-Mode leads to a reduction of the ELM induced energy fluence $\epsilon_{||}$. The reduction of the $\epsilon_{||}$ is correlated to the observed reduction of the pedestal pressure. The energy fluence in both phases with and without external magnetic perturbation is described by a model using the pedestal pressure a main ordering parameter [22]. Future ELM mitigation studies need to correct for the loss in pedestal pressure in order to asses ELM mitigation.

Acknowledgement

This work has been carried out within the framework of the EUROfusion Consortium and has received funding from the Euratom research and training programme 2014-2018 under grant agreement No 633053. The views and opinions expressed herein do not necessarily reflect those of the European Commission.

References

[1] LOARTE, A. et al., Plasma Physics and Controlled Fusion **45** (2003) 1549.

[2] LANG, P. et al., Nuclear Fusion **53** (2013) 043004.

[3] LOARTE, A., Nuclear Fusion **54** (2014) 033007.

[4] SIEGLIN, B. et al., Plasma Physics and Controlled Fusion **58** (2016) 055015.

[5] EICH, T. et al., Phys. Rev. Lett. **107** (2011) 215001.

[6] FAITSCH, M. et al., Plasma Physics and Controlled Fusion **?** (2016).

[7] MAKOWSKI, M. A. et al., Physics of Plasmas (1994-present) **19** (2012) 056122.

[8] SCARABOSIO, A. et al., Journal of Nuclear Materials **438, Supplement** (2013).

[9] EICH, T. et al., Nuclear Fusion **53** (2013) 093031.

[10] SIEGLIN, B. et al., Plasma Physics and Controlled Fusion **55** (2013) 124039.

[11] SCARABOSIO, A. et al., Journal of Nuclear Materials (2014) .

[12] FAITSCH, M. et al., Plasma Physics and Controlled Fusion **57** (2015) 075005.

[13] SUTTROP, W. et al., Fusion Engineering and Design **84** (2009) 290 .

[14] SUTTROP, W. et al., Phys. Rev. Lett. **106** (2011) 225004.

[15] TESCHKE, M. et al., Fusion Engineering and Design **9697** (2015) 171 .

[16] ROTT, M. et al., Fusion Engineering and Design **9899** (2015) 1144 .

[17] SIEGLIN, B. et al., Review of Scientific Instruments **86** (2015).

[18] JAKUBOWSKI, M. et al., Journal of Nuclear Materials **415** (2011) S901 .

[19] NARDON, E. et al., Journal of Nuclear Materials **415** (2011) S914 .

[20] CAHYNA, P. et al., Journal of Nuclear Materials **438, Supplement** (2013) S326 .

[21] MLLER, H. et al., Journal of Nuclear Materials **438, Supplement** (2013) S64 .

[22] T.EICH et al., **Submitted** (2016).

[23] KIRK, A. et al., Nuclear Fusion **55** (2015) 043011.

[24] RACK, M. et al., Nuclear Fusion **54** (2014) 064012.